Chapter 41
Torque Ripple Reduction of a Solar PV-Based Brushless DC Motor Using Sliding Mode Control and H7 Topology

D. V. N. Ananth and D. A. Tatajee

Abstract In this paper, the solar PV-based brushless DC motor (BLDC) torque ripple reduction is reduced using sliding mode control algorithm and H7-based inverter topology. In general, the outer speed control loop of a BLDC motor is controlled using a well-tuned PI controller. This controller will be effective in reducing the dynamic speed error, but will produce large current ripples. This reference current when given to the inner control loop and controlled using Hall effect position sensing technique leads to comparatively large ripples in the torque. Hence, to mitigate this torque ripples in solar PV-based BLDC motor, sliding mode controller is used, which is designed in such a way that, it will effectively control the speed and also produces lesser current ripples reference. Further, the inverter topology uses a seven switch H7 configuration instead of a conventional six switch inverter topology. The results are compared with a PI-based converter with a six switch under variable load torque and variable speed cases in MATLAB/SIMULINK environment. The BLDC motor is used as a drive for the electrical transportation vehicle, and performance is observed. It is found that, the torque ripples are reduced effectively without much change in the reference speed. Also, even at lower speeds, the torque ripples and surges are also lesser.

Keywords Brushless DC (BLDC) motor · Current and torque control · Torque ripples reduction · Field-oriented control · Sliding mode control · Electrical vehicle for transportation

D. V. N. Ananth (✉)
Department of Electrical and Electronics Engineering, Raghu Institute of Technology, Visakhapatnam, India

D. A. Tatajee
Department of Electronics and Communication Engineering, Vignan's Institute of Engineering for Women, Visakhapatnam, India

P. V. Baredar et al. (eds.), *Advances in Clean Energy Technologies*,
Springer Proceedings in Energy, https://doi.org/10.1007/978-981-16-0235-1_41

41.1 Introduction

The brushless DC motor (BLDC) is slowly replacing the most popular induction motor due to its advanced control techniques and design improvements. This is due to the fact that, BLDC motors are attractive now days due to its lower cost, higher efficiency, low cost, lesser maintenance, high torque, and speed control capabilities compared to the other same class of motors [1, 2]. This motor is controlled based on the position of the rotor and is estimated by using hall sensors or using some sensor-less techniques. This BLDC motor finds applications in computers, automotive, households, industries, railway fans, household, and many. The BLDC motor is used in automotive industry [3], solar PV-fed system [4], and electrical vehicle applications [5], as a turbocharger [6], aerospace vehicle [7], fuel pumps [8], and many.

The BLDC motor speed and torque control are very important for effective performance based on the application [9–14]. The authors used effectively demonstrated the fuzzy-PID along with model-reference adaptive control technique in the outer control loop of BLDC is a better speed control [9] technique. Earlier in [10], such speed control is done using a neuro-fuzzy system with weights being adjusted using BAT-based metaheuristic algorithm. However, these two methods are very effective, but are very complicated. There are various methods adopted for BLDC for higher speed operation [11] or for very low speed operation as in [12] or variable speed control as in [13]. The torque control is achieved using many methods and among them one such method is in [14] using a firefly algorithm to tune the PID control parameters for better operation.

The speed, torque, or power control for BLDC are obtained using famous algorithms like direct power control [15, 16], direct torque control [17, 18], field-oriented control technique [19, 20], and hybrid direct torque and field-oriented control technique [21]. Among all, the hybrid technique which uses both stationary and rotating reference frames is found to be more feasible and attractive solution for performance improvement of BLDC. The major challenges for BLDC motor for any type of application are torque ripple reduction [22–24]. The torque ripples will deteriorate the performance, efficiency, commutation, and controllability of the motor. Hence, such challenge is very crucial for most of the applications.

The BLDC motor is controlled using different control schemes to achieve rapid and required speed, torque, power, or stability [25–29]. The authors in [25, 26] Premkumar, and Manikandan have done a great work in identifying different controllers for speed control and stability enhancement using fuzzy and many hybrid metaheuristic and intelligent control schemes. Similarly, h-infinity [27], fuzzy-PSO controller [28], and adaptive sliding mode control and cuckoo method [29] is used by these authors for lifetime and performance improvement. Therefore, the choice of the controller other than a conventional PI controller is important for improving the motor performance.

Different converter topologies like SEPIC and three-level neutral point converter [30] are used for torque ripple reduction, DTC and overlap angle method in [31],

Z-source inverter [32], quasi-square wave inverters [33] and Cuk, SEPIC and Zeta converter [34]. The later papers deal with both the torque ripples reduction and power factor correction. Based on the converter topology and control scheme adopted, the performances like torque and speed control, torque ripples reduction, and power flow control are improved considerably.

This paper deals with sliding mode controller scheme with H7 inverter topology for speed and torque control along with torque ripple reduction. The same topology with same motor ratings is tested for electrical vehicle application with battery energy storage system to observe the effectiveness under this type of application. Also, with the present topology, very high load torque at high speed operation is planned. The objectives of the work are torque surges must be low when there is a rapid change in the speed and also the torque ripples must be low when speed of the rotor is adjusted at very low or higher speeds. The control scheme has to be simple and effective and can be applicable to any application like pumps, automotive, or aerospace.

The objectives of the work are described as below:

1. To integrate solar PV power generation to a BLDC motor drive system without transfer for boost voltage application.
2. To develop improved topology without the transformer using the H7 configuration.
3. To reduce the leakage current utilizing the parasitic capacitor already present in the circuit and also the effects due to inductors, diodes, and solid-state switches.
4. Establishing a bidirectional current flow to aid in charging and discharging because of energy storage devices with the already available DC link capacitor.
5. Use of sliding mode control for effective control and improved performance than conventional PI controller.
6. Multi-level voltage levels are developed to improve the THD and voltage profile for BLDC motor drive connection.
7. System is tested for an application of the BLDC motor for an electrical vehicle load drive application where its load is very intermittent and disturbing in nature.

Section 41.2 of this paper discusses the modeling and control of solar PV-based BLDC motor in state space representation with current, position, and speed as variable parameters. Section 41.3 describes the sliding mode control strategy and H7 topology for BLDC motor for speed control. Section 41.4 explains the control strategy of the inverter and SMC technique adopted. Results and discussions are demonstrated in Sect. 41.5 for the test system under four cases like constant speed and variable torque and variable speed and constant torque operation and another case with same motor topology and control scheme for electrical vehicle application. Finally, Sect. 41.6 concludes the work followed by appending showing the parameters of the system and then the references.

41.2 Mathematical Modeling of BLDC Motor

The modeling of SMC will be considering the dynamics of BLDC motor to achieve better speed and torque control. The FOC decoupling is referred in stator flux frame with the basic relationships which can be represented as [3, 9, 11, 20, 24, 29]. The d- and q-axis stator voltages of BLDC motor are given by Eqs. (41.1a and 41.1b)

$$V_d = Ri_d + \rho\lambda_d - \omega_r\lambda_q \tag{41.1a}$$

$$V_q = Ri_d + \rho\lambda_q + \omega_r\lambda_d \tag{41.1b}$$

where R is the stator resistance, ρ is the differential equation $\frac{\mathrm{d}}{\mathrm{d}t}$, d- and q-axis flux is given by λ_d and λ_q with rotor angular speed given by ω_r. The d- and q-axis stator flux linkage is given Eqs. (41.2a and 41.2b) in terms of d- and q-axis stator current i_d and i_q, mutual flux linking toward the rotor Ψ_R and stator inductance L_s is

$$\lambda_d = L_\mathrm{s}i_d + \psi_\mathrm{R} \tag{41.2a}$$

$$\lambda_q = L_\mathrm{s}i_q \tag{41.2b}$$

The electromagnetic torque (EMT) (T_e) in terms of d- and q-axis flux and current and also in terms of mechanical parameters is represented in Eq. (41.3).

$$T_\mathrm{e} = \frac{3}{2}\left(\lambda_d i_q - \lambda_q i_d\right) = \frac{3}{2}\psi_\mathrm{R} i_q = \frac{3}{2}\frac{P}{2}\lambda_\mathrm{m} = \frac{JP}{2}\dot{\omega}_\mathrm{r} + \frac{3\rho}{2}\omega_\mathrm{r} + T_l \tag{41.3}$$

The λ_m is the flux linking component in the permanent magnet rotor, and T_l is the load torque and P is pole pairs. The d- and q-axis stator voltage can be derived in terms of current and Ψ_R using Eqs. (41.1a–41.2b) is given by (41.4a and 41.4b) equations. It can be observed that there are decoupling current parameters in the voltage, and hence, d- or q-axis current will effectively influence both d- and q-axis voltages and effective control of this current will result in driving the BLDC motor based on the requirement.

$$V_d = Ri_d + L_\mathrm{s}\rho i_d + \rho\psi_\mathrm{R} - \omega_\mathrm{r}L_\mathrm{s}i_q \tag{41.4a}$$

$$V_q = Ri_q + L_\mathrm{s}\rho i_q + \omega_\mathrm{r}\psi_R + \omega_\mathrm{r}L_\mathrm{s}i_d \tag{41.4b}$$

The Ψ_R flux is constant due to permanent magnet of the rotor, and therefore, the rate of change of Ψ_R is zero. Under stationary rotor condition, the angular speed ω_r is zero. Hence, the d- and q-axis rate of change of currents in terms of d- and q-axis voltages as shown in equations (41.5)

$$\frac{V_d - Ri_d}{L_E} = \frac{\mathrm{d}i_d}{\mathrm{d}t} \text{ and } \frac{V_q - Ri_q}{L_s} = \frac{\mathrm{d}i_q}{\mathrm{d}t} \tag{41.4c}$$

Upon solving Eq. (41.4c), the simplified d- and q-axis currents at standstill rotor condition are given by Eq. (41.4d). The d- and q-axis depends on the stator time constant $\tau = \frac{L_s}{R}$,

$$i_d = \frac{V_d}{R}\left(1 - \mathrm{e}^{-\frac{R}{L_s}t}\right) \text{ and } i_q = \frac{V_q}{R}\left(1 - \mathrm{e}^{-\frac{R}{L_s}t}\right) \tag{41.4d}$$

In the same way, if the d- and q-axis currents and flux are controlled effectively to get the desired EMT and mostly q-axis current will be more dominating in the field-oriented control. In this regard, to achieve better control of this EMT, the q-axis current control plays a vital role. Compared to a conventional standard PI controller, a nonlinear controller like SMC will influence this q-axis current flow in a better way.

41.3 Modeling of SMC for BLDC Performance Improvement

The SMC is technique provides an efficient and high switching frequency control with more uncertainties in the nonlinear system [16, 29]. The SMC technique is mostly applied for BLDC motor controlled using DTC with flux or torque control. In this paper, the SMC is applied for FOC with hysteresis control to have good current control output and lesser torque ripples. The SMC is designed in such a way that the output current profile has to change when there is change in rotor speed and also its rate of change in the speed of the rotor has to be controlled effectively. Hence, the speed error, reference speed, and rate of change in rotor speed are considered as controllable variables here.

Equation (41.3) can be written as

$$\dot{\omega}_\mathrm{r} = -C_1\omega_\mathrm{r} + C_2 i_q - C_3 T_\mathrm{l} \tag{41.5}$$

where $C_1 = \frac{B}{J}$, $C_2 = \frac{\rho}{2J}\frac{3P}{2*2}\lambda_\mathrm{m} = \frac{3\rho P}{8J}\lambda_\mathrm{m}$ and $C_3 = \frac{P}{2J}$.

The uncertainties in the dynamic speed equation is represented as

$$\dot{\omega}_\mathrm{r} = -(C_1 + \Delta C_1)\omega_\mathrm{r} + (C_2 + \Delta C_2)i_q - (C_3 + \Delta C_3)T_\mathrm{l} \tag{41.6}$$

The ΔC_x parameters are the uncertainties of the respective expressions for $x = 1$, 2, and 3.

The tracking speed error is

$$e(t) = \omega_\mathrm{r}(t) - \omega_\mathrm{r}^*(t) \tag{41.7}$$

where the $\omega_r^*(t)$ is the rotor speed reference or command to get the desired rotor speed. Equation (41.6) can be rewritten as to the dynamic speed error $e(t)$ as shown in Eq. (41.8a)

$$\dot{e}(t) = -C_1 e(t) + C_2 i_q - C_3 T_l - \Delta C_1 \omega_r + \Delta C_2 i_q - \Delta C_3 T_l \tag{41.8a}$$

This Eq. (41.8a) is represented in the control signal $u(t)$ and uncertainty signal $d(t)$ as

$$\dot{e}(t) = -C_1 e(t) + u(t) + d(t) \tag{41.8b}$$

The control signal

$$u(t) = -C_3(t) + C_2 iq(t) - C_1 \omega_r^*(t) - \dot{\omega}_r(t) \tag{41.8c}$$

The uncertainty signal term

$$d(t) = -\Delta C_1 \omega_r(t) + \Delta C_2 i_q(t) - \Delta C_3(t) \tag{41.8d}$$

Now the sliding surface variable is designed and can be represented using $S(t)$ which includes the integral component as given by Eq. (41.9) using the reference paper [35] as

$$S(t) = e(t) + \int_0^t (K + C_1) e(\tau) \mathrm{d}\tau \tag{41.9}$$

where K is the gain constant, the design of SMC as per the law is shown in Eq. (41.10) as

$$u(t) = -K e(t) - \beta \mathrm{sgn}(S) \tag{41.10}$$

With the β as the switching variable and the S is sliding variable and sgn(S) is the signum function.

The following assumptions are considered in order to ensure the desired tracking error with gain K is chosen such that $K + C_1$ is strictly positive or K has to be greater than $-C_1$ and the switching variable (β) also has to be greater than or equal to the disturbance variable term $|d(t)|$ for all the values of time 't'.

Under the sliding mode state $S(t) = \dot{S}(t) = 0$ and so the tracking problem dynamic behavior with the speed tracking error from Eq. (41.7) is equally governed. Equation (41.9) will now become as in Eq. (41.11) with the sliding mode state condition as

$$\dot{e}(t) = -(K + C_1) e(t) \tag{41.11}$$

and the desired current command can be obtained when using Eqs. (41.8c) and (41.10) as

$$i_q^* = \frac{1}{C_2}\left\{Ke + \beta \text{sgn}(S) - C_3 - C_1\omega_r^* - \dot{\omega}_r^*\right\} \tag{41.12}$$

Therefore, the current output from the SMC with the speed control is given by the expression as shown in Eq. (41.12) which depends on the sgn(S), error in the rotor speed, rotor speed reference and change in the rotor speed. Also, it is dependent on the constant C_1, C_2, and C_3 as well as the constants K and β. The K and β values are obtained based on the assumptions discussed above. The H7 topology is considered based on the reference paper [36] which is developed for solar PV inverter, but here used for the BLDC motor with a different converter switching technique.

If the d- and q-axis voltages are controlled using a conventional standard PI controller, these voltages can be represented as

$$V_d = PI\left(i_d^* - i_d\right) - \omega_\text{r} i_q \text{ and} \tag{41.13}$$

$$V_q = PI\left(i_q^* - i_q\right) + \omega_\text{r} i_d + \frac{\lambda_\text{m}}{L}\omega_\text{r} \tag{41.14}$$

41.3.1 Power Losses Calculations

Any motor power losses are broadly classified as core (P_core) and copper (P_CU) losses. The copper power losses are variable losses, and these losses increase with the increase in the winding current produced BLDC motor. It is a function of summation of all phases and fundamental to all phases RMS current represented as shown in Eq (41.15). Here, I_{a_i} is the i**th** harmonic current component of a-phase called I_a. The core losses in the BLDC motor are a function of hysteresis (P_h) and eddy current losses (P_e) which are functions of eddy current constant (K_e), hysteresis current constant (K_h), frequency (f), maximum flux density (B_max), and its weight as depicted by Eq. (41.16).

$$P_\text{Cu} = 3R\sqrt{\sum_{i=1}^{\infty} I_{a\_i}^2} \tag{41.15}$$

$$P_\text{core} = P_\text{e} + P_\text{h} \cong \left(k_\text{e} f^2 B_\text{max}^2 + k_\text{h} f B_\text{max}^2\right) * \text{Weight} \tag{41.16}$$

The total eddy current losses to the fundamental eddy current losses is represented by Eq. (41.17) and similarly for hysteresis losses is shown in Eq. (41.18). These losses are dependent on the RMS of all the voltages from the fundamental to the infinite

harmonics existing in the network to the fundamental harmonic voltage. Hence, the parameter is always greater than equal to one.

$$\frac{P_{\mathrm{e}}}{P_{\mathrm{e1}}} = \sum_{i=1}^{\infty} \left(\frac{V_i}{V_1}\right)^2 \tag{41.17}$$

$$\frac{P_{\mathrm{h}}}{P_{\mathrm{h1}}} \approx \sum_{i=1}^{\infty} \left(\frac{V_i}{V_1}\right)^2 \frac{1}{i} \tag{41.18}$$

The resistance and inductance and all the constants and coefficient values are taken at room temperature and pressure. These two equations help us to evaluate the losses occur in the BLDC motor and the harmonic injection values.

41.4 SMC and H7 Inverter Control Strategy for Speed, Torque Control, and Ripples Reduction

The complete bock diagram for the BLDC motor control scheme is shown in Fig. 41.1. The control circuit is developed for effective speed and torque control with minimum torque ripples. To achieve this, sliding mode control (SMC) scheme and H7 inverter topology are adopted with the operation as described in Sect. 41.3. The SMC is designed to track the speed error input and to maintain it to lowest value (zero) and the output current reference with an aptitude with least possible ripples. The H7 inverter is developed to produce trapezoidal emf with speed and torque control. The complete block diagram of the BLDC control circuit is shown in Fig. 41.1a. The speed of the rotor is the input, and the seven switching pulses ($S1$–$S7$) are output for this figure.

Here, the reference speed (N_{ref}) and actual speed (N) are compared, and the speed error signal (en*) is given to the SMC to get reference DC current called (I_a^*). The actual DC current is the current passing through the H7 switch (I_H7), and this reference current I_a^* is compared and the current error (e_Ia) is given to the hysteresis controller. The output of this hysteresis controller is three-phase reference currents (I_{abc}) block diagram which is shown in Fig. 41.1b. The rotor position is sensed by the Hall effect sensor and will give reference back-emf (E_abc*). This is a conventional method to achieve the reference back-emf voltage. The Hall effect sensor-based switching working scheme is shown in Table 41.1. The reference three-phase currents and reference back-emf are given to the pulse generator to get the seven pulses for the respective switches, and its internal block diagram is shown in Fig. 41.1c.

The hysteresis current control scheme internal block diagram is shown in Fig. 41.1b. Here the I_a^* is the reference current obtained from SMC output, and bias is a constant value. The error current signal is e_Ia along with I_a^* and bias are compared with zero signal and logic technique to get the reference three-phase

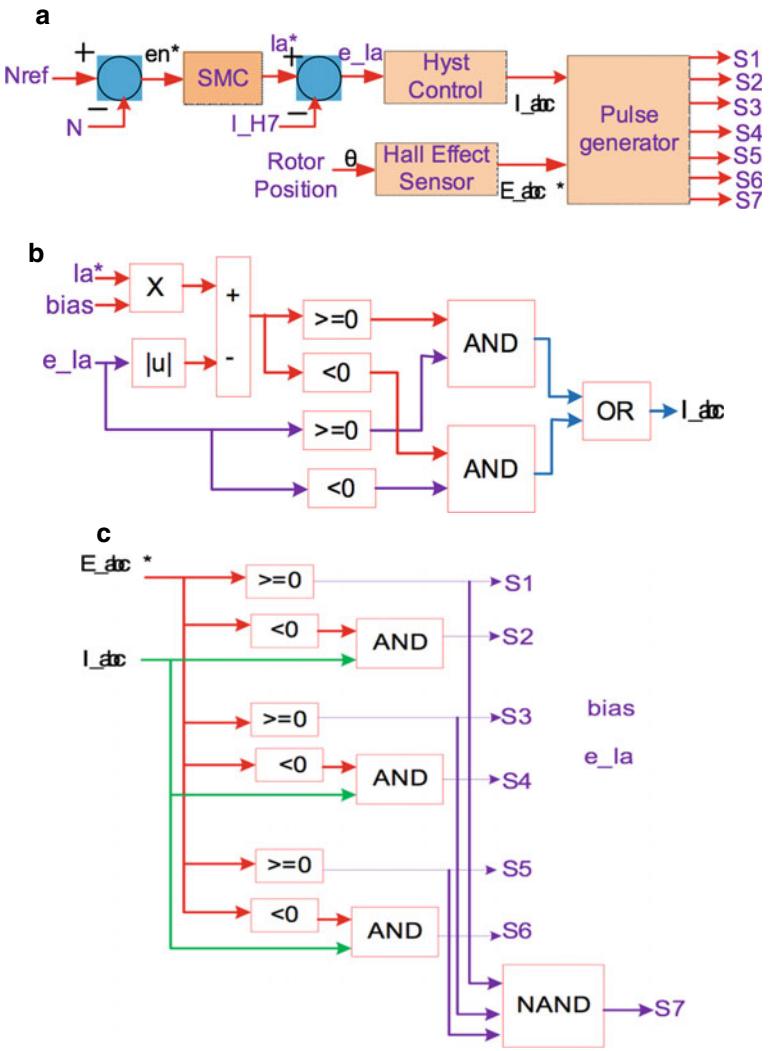

Fig. 41.1 **a** Control circuit of BLDC motor for torque ripple reduction. **b** Hysteresis current control scheme. **c** Pulse generator internal circuit block diagram. **d** SMC block diagram. **e** Block diagram of solar PV-based BLDC speed and torque control scheme using SMC and H7 inverter

current. The seven IGBT pulses will be getting pulses using the reference back-emf voltage E^*_{abc} and reference hysteresis controller current I_{abc} by comparing them as shown in Fig. 41.1c. The internal block diagrams in Fig. 41.1b, c are self-explanatory. The switching logic table for the pulse generation scheme for the seven switch inverter scheme is shown in Table 41.2.

Based on the back-emf input value, the switching On and Off is decided based on this mechanism. The SMC internal block diagram is shown in Fig. 41.1d, and

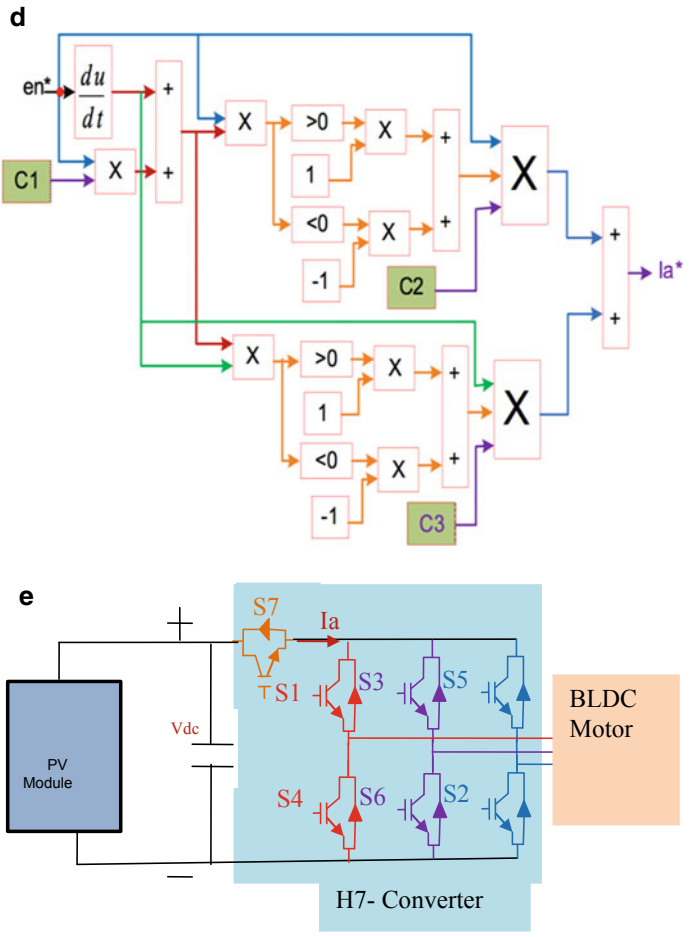

Fig. 41.1 (continued)

Table 41.1 Hysteresis block working table

Ha	Hb	Hc	EMF_a	EMF_b	EMF_c
0	0	0	0	0	0
0	0	1	0	−1	+1
0	1	0	−1	+1	0
0	1	1	−1	0	+1
1	0	0	+1	0	−1
1	0	1	+1	−1	0
1	1	0	0	+1	−1
1	1	1	0	0	0

Table 41.2 Pulse generator switching table

EMF_a	EMF_b	EMF_c	S1	S2	S3	S4	S5	S6	S7
0	0	0	0	0	0	0	0	0	0
0	−1	1	0	0	0	1	1	1	1
−1	1	0	0	1	1	0	0	0	1
−1	0	1	1	0	0	0	0	1	1
1	0	−1	0	1	0	0	1	0	1
1	−1	0	1	0	0	1	0	0	1
0	1	−1	0	0	1	0	0	1	1

the MATLAB design of the test system under consideration is shown in Fig. 41.1e. The *en** is the speed error input value. Let output of the differential value is assumed as *A*, and the output of the first left corner summer is assumed as *B*. Then the SMC control technique works as follows. There are three bias constants which controls the sliding surface of SMC and control the input to the SMC to attain zero value quickly and are called here as $C1$, $C2$, and $C3$. The output of the top right summer is represented as $X1$ and bottom right summer output as $X2$. The multiplication parameter is represented here with '*x*', then

*en** = error in speed value, $A = \frac{\mathrm{d}}{\mathrm{d}t}(en*)$, $B = C1 \times (en^*) + \mathrm{A}$. The logic table of Fig. 41.1d is, if the $B * (en^*)$ is greater than zero, then $X1$ is 1, else it is -1. Similarly, if the output of $B * A$ is greater than zero, then $X2$ is 1, else it is -1. The output is current reference $= C2 \times (en^*) \times X1 + C3 \times A \times X2$.

41.5 Results and Discussion

The performance of solar PV-based BLDC motor system with conventional sensor-based BLDC system with field-oriented control logic and PI-based speed error controller is compared with the proposed sliding mode control (SMC)-based speed controller with the help of seven switches H7 topology which is considered for the analysis. The speed and torque control along with speed and torque ripples are considered for the analysis. The BLDC parameters like armature one phase current, back-emf of the same phase, load torque and electromagnetic torque (EMT), reference and actual speed, and DC link capacitor voltage are compared for the analysis. Further inverter three-phase voltage and current, PI and SMC input and output waveforms are also considered to show the efficacy of the proposed work. The observed under two cases, with the first case with constant speed and variable torque control and the second case with constant torque and variable speed control.

41.5.1 *Case A: Constant Speed and Variable Torque Control of BLDC Motor*

In this, the solar PV-based BLDC motor is operated under constant speed at 1500 rpm, and load torque is varying from 15–30 N m at 0.05 s, later to 40 N m at 0.1 s and finally to 60 N m at 0.15 s. The waveforms for the conventional control scheme with PI controller and proposed SMC-based H7 inverter configuration are shown from Figs. 41.2, 41.3 and 41.4. In Fig. 41.2a, b, the BLDC motor parameters and DC link capacitor voltage are shown with PI and SMC scheme. The BLDC A-phase stator current using conventional technique is having distorted trapezoidal waveform with notches as shown in Fig. 41.2a (top) while with SMC, the current waveform is trapezoidal as shown in Fig. 41.2b (top). The stator current can be observed to be increasing with increase in the load torque. When compared with the conventional and proposed techniques, the back-emf decreased when load is increased to 60 N m with conventional technique, whereas with the proposed technique, this voltage is constant in amplitude. Hence, developed torque is sufficient to carry the increased load demand on the motor effectively with the proposed technique.

The reference load torque is shown in black line, and actual electromagnetic torque (EMT) is shown in red color waveform for both conventional and proposed techniques. It is observed that the starting EMT surges are almost same for both the techniques and this sub-transient surge is observed till the motor reaches its desired speed. It can be observed that, there are more ripples in the torque waveform with conventional technique. With the conventional technique, when the reference torque is set at 15 N m, the EMT is varying from 0 to 25 N m from starting till 0.05 s. When

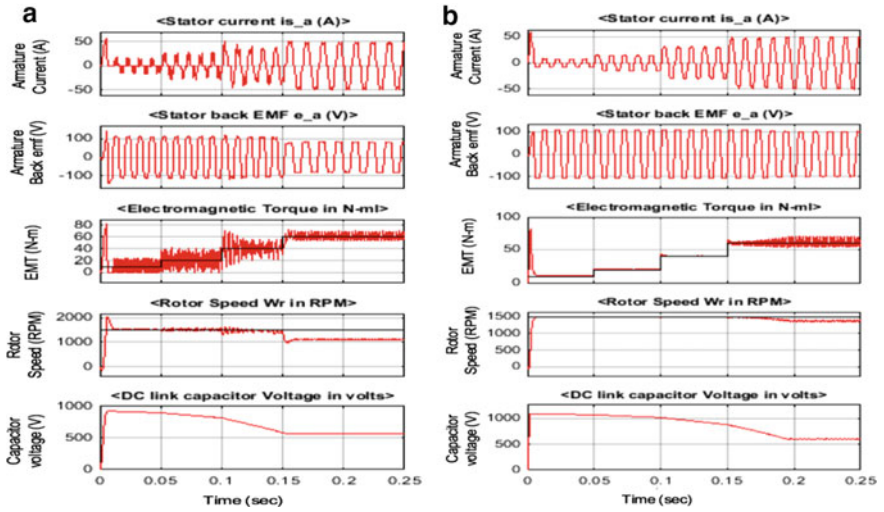

Fig. 41.2 **a** Solar PV-based BLDC motor parameters and DC link capacitor voltage with PI controller, **b** with SMC under constant speed and variable torque case study

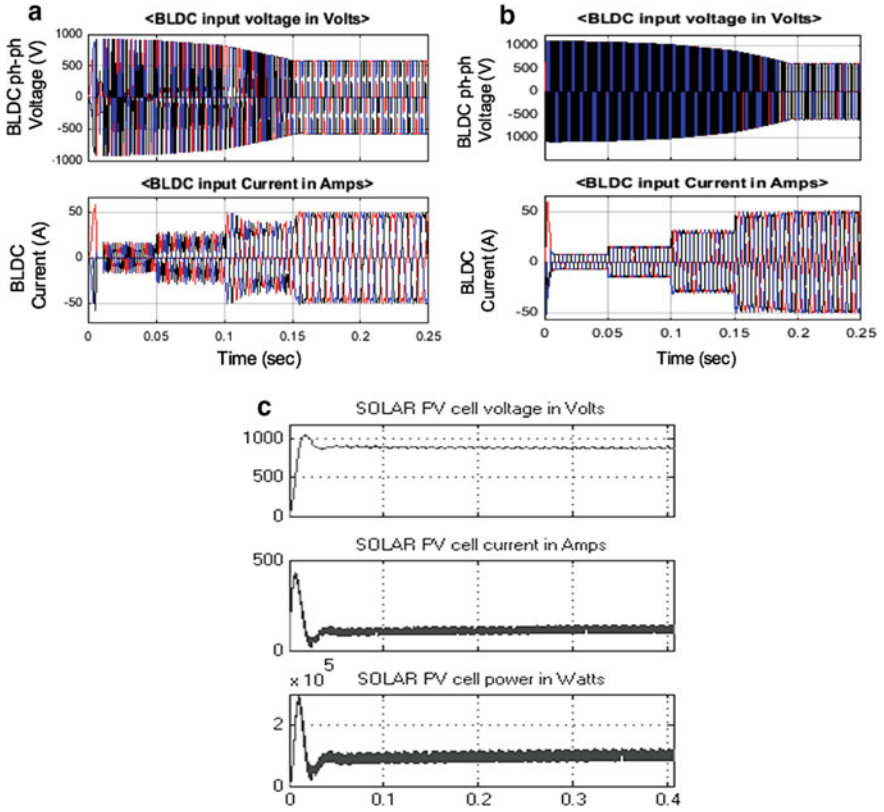

Fig. 41.3 **a** Solar PV-based BLDC motor inverter voltage and current with PI controller, **b** with SMC. **c** Solar PV cell output voltage, current, and power waveforms

the reference load torque changed to 30 N m at 0.1 s, this EMT is fluctuating from 20 to 40 N m. Similarly, the EMT is varying from 63 to 27 N m when load torque shifted to 40 N m. The ripples slowly decreased with the range from 30 to 50 N m. Now at 0.15 s, this load torque increased suddenly to 60 N m; during this period, the surges are lesser at this load with variation from 50 to 70 N m. Hence, there are more surges with this control scheme. The reason for large ripples is due to the fact that the output of PI controller is having large ripples as shown in Fig. 41.4a. The current ripples are very high till 0.15 s, so torque ripples are also high. The same dynamic analysis for the EMT is analyzed when SMC with H7 inverter is used.

The starting surge is almost same for both techniques but the ripples are very less when the load torque is up to 40 N m. But, when this load torque increased to 60 N m, there are few ripples observed in this from 0.15 s. This is because the motor is extracting more current from the stator to drive this heavy load. But due to permanent magnet behavior of rotor, more decomposition of flux is difficult to obtain. However, with the proposed technique, the ripples are comparatively less.

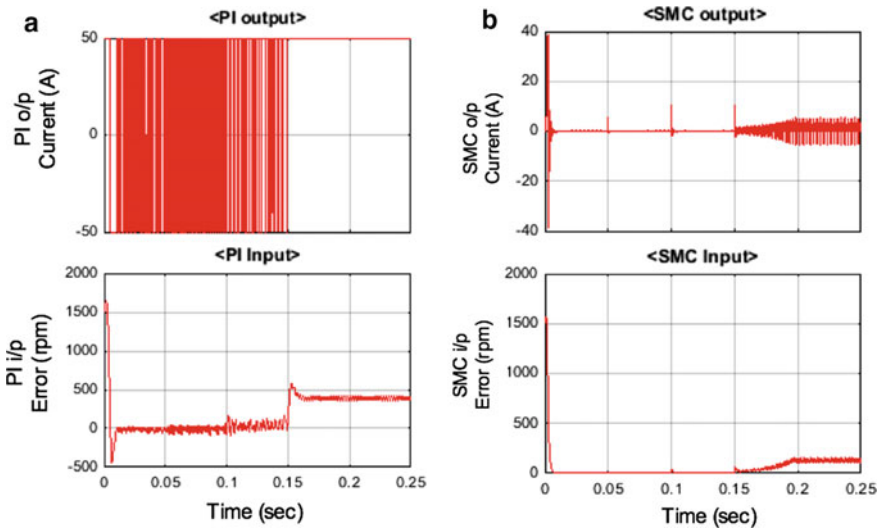

Fig. 41.4 **a** Output current and input speed error with PI controller, **b** with SMC

Also can be observed from Fig. 41.4b, the SMC output is having lesser ripple when load torque is low, but this rippled got increased considerably when load torque is increased to 60 N m.

The rotor speed with both control schemes is shown here under variable load torque and constant speed case study. There is an overshoot in the rotor speed with conventional technique and also few sustained oscillations observed when the load torque is changing suddenly at 40 N m. When the load suddenly increased to 60 N m, the speed of the rotor is decreased from reference 1500–1100 rpm due to decrease in the back-emf developed. So, with increase in the load above 45 N m which is 75% rated value, there is a droop in the speed curve due to the permanent magnet behavior of the rotor and control circuit unable to supply desired back-emf. With the SMC technique, the rotor speed is almost constant at desired 1500 rpm all load reaches 40 N m value. When suddenly load torque increased to 60 N m, this rotor speed drooped but the slip in the speed value changed from desired 1500–1400 rpm. Hence in terms of speed control and torque control, the proposed method is advantageous with better performance in all aspects. The performance of proposed technique is comparatively improved when compared with the latest works in [30, 31].

When the DC link voltage across the capacitor is observed for both the techniques, with increase in the load torque, the DC link voltage is decreasing for both the cases, but this droop is considerably high with conventional PI control scheme than with SMC. Initially at 15 N m load torque, the DC link voltage is 900 V for conventional and 1100 V for proposed. This voltage is decreased slowly to 800 V when torque increased o 30 N m for conventional and 1000 V for proposed. When load further increased to 40 N m, the voltage decreasing further slowly to 550 N m with conventional and 900 V for proposed. When load finally reached to 60 N m,

the DC link voltage is constant at 550 V with conventional from 0.15 s, but with the proposed, this capacitor voltage decreased slowly to 550 N m for few seconds and later remained constant at 550 V.

The inverter voltage and current waveforms for this case with conventional control scheme with PI controller and proposed SMC-based H7 inverter configuration are shown in Fig. 41.3a, b. The voltage waveform is distorted and not trapezoidal of constant amplitude with conventional scheme. Here the voltage is fluctuating and decreasing with increasing in the load value due to the change in the capacitor voltage value. At light load, the inverter voltage is 800 V and decreased to 600 V phase to phase. But when the torque increased to 60 N m, the DC link voltage remained constant at 600 V and the waveform got better. This is due to the change in the capacitor voltage value and also because of the PI output current ripple value. The current waveform is also having similar distortions with conventional technique.

When the same voltage and currents are observed with the proposed H7 inverter topology, the voltage waveform is having same amplitude under same load torque as capacitor voltage is almost constant as shown in Fig. 41.2b bottom right. But when the load torque is increased to rated value of 60 N m as shown in Fig. 41.3b, which is often the case, there is a decrease in the inverter voltage due to decrease in the capacitor link voltage. But the current three-phase waveform is constant when the load is constant, but is increased and maintained constant in aptitude as load torque is increased. When the load is at 15 N m, the current is 8 A, and increased to 17 A when load increased to 30 N m. This current further increased to 30 A when the load reached 40 N m, and finally, when the load became 60 N m, the inverter current is 51 A. The distortions in current and voltage waveforms are lesser with the proposed control scheme. The solar cell output voltage, output current, and MPPT-based output power waveforms are in Fig. 41.3c. For analysis, the irradiation is assumed to be constant and id operating under normal conditions with good sunlight without shading and Perturb and Observer-based MPPT algorithm. The solar PV output power is assumed to be constant at 850 volts and current can vary based on load and irradiation between 100 and 150 A with. The power output in the solar PV cell is considered to be 150 kW.

The output and input of PI controller are shown in Fig. 41.4a and with SMC is shown in Fig. 41.4b for the same case. When considering the PI controller case, initially rotor speed is increasing from zero to 1500 rpm. So, rotor rotated in opposite direction at the beginning for little time started to rotate in forward direction. Hence, the PI error input value started from 1550 value and decreasing. With PI controller, the rotor speed increased beyond 1500 rpm for few seconds, so the PI error input extended to −400 values and settled at near zero value later at the load of 15 N m. The reason for the overshoot or undershoot is because of the integral parameter constant value. If this value is decreased, the settling time will be increased which is not desired in general for a BLDC motor for general applications. The speed error or input to the PI controller is controlled effectively with well-tuned PI controller. But, when the load increased to higher values the PI controller behavior got disturbed and hence there is a diversion in error value. The PI controller output is current reference. If it is observed that PI input is well controlled, but output is having large fluctuations.

The PI saturation block limits helped to control the current to 50A peak to peak. With SMC, the input is speed error and output is reference current like the PI controller as shown in Fig. 41.4b. It can be observed that the error value is maintained almost to zero value till the load is 40 N m and a small deviation of 100. The SMC output is maintained at small value, but some surges are observed when load changes take place. This SMC will track the reference and actual speeds and will effectively limit this as this is a very fast active device than a PI controller. However when load change is very high, that is at 60 N m, the SMC output is also having ripples but are smaller compared to PI.

Hence from this case study, it can be understood that, the SMC performance is very superior to PI controller in maintaining the speed and controlling the torque. The torque ripples are minimized, torque and speed surges are curtailed, and overall performance is improved. With the proposed technique, heavy load can be operated effectively on a BLDC motor while maintaining the speed almost constant. In the next subsection, the case study is variable speed and constant load operation.

41.5.2 Case B: Constant Torque and Variable Speed Control of Solar PV-Based BLDC Motor

In the earlier case, constant speed variable torque is discussed, now variable speed and constant torque will be considered. A half load of 30 N-m is fixed, and speed reference is changed from 1000 to 1750 and 2500 rpm at 0.075, and 0.15 s, respectively. The machine parameters and other are remained same as in the earlier case. The starting current with PI controller is 50 A and with SMC is 62 A, and this initial current settled once the solar PV-based BLDC motor reaches steady-state reference value. It can be observed with conventional method that, at low load torque and low speed, the armature current is distorted with spikes and notches as shown in Fig. 41.5a. But with the SMC as shown in Fig. 41.5b, the current is trapezoidal and amplitude is almost constant and few negligible surges in the current are observed when the speed changes from one value to the other. In both the cases, the frequency of the current waveform is increasing as speed is increasing. The back-emf is almost trapezoidal with both technique, and this voltage is increasing with increase in the rotor speed.

The ripple in the torque is high with PI and varies from 0 to 50 N m when the speed is lesser at 1000 rpm. The distortions decreased with increase in speed and are less as speed increased to a higher value. In the same way, the torque ripples are lesser at lower speed with SMC and almost same as reference and actual torque. But few surges are observed when the speed adjustment is done as due to change in the SMC input and output values as speed is changed. When the reference and actual speed is compared with both controllers, there are few overshoots and controlled oscillations are observed when speed transient take place for PI controller. But when the speed is increased to a higher value at 2500 rpm, the rotor cannot adjust to the desired speed and attained only 2000 rpm.

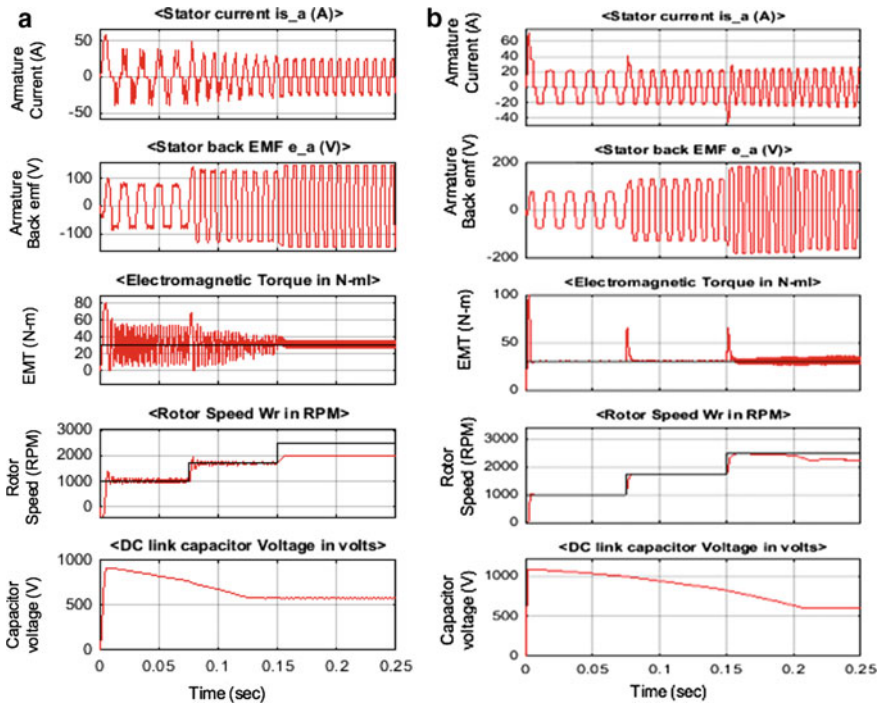

Fig. 41.5 **a** BLDC motor parameters and DC link capacitor voltage with PI controller, **b** with SMC under constant torque and variable speed case study

The SMC-based technique output is observed, the reference and actual speeds are almost same for speeds up to 1750 rpm, but a deviation of about 250 rpm is observed with SMC which is comparatively lesser in deviation than with the PI controller. The DC capacitor value which is chosen some small value in this paper deviated from lesser speed value to higher speed value in both the cases. But, this voltage is maintained constant for more time with the rapid change in the speed with SMC. If higher value of capacitor is chosen, the capacitor link voltage is maintained constant; hence, speed deviation can be curtailed for both the cases. However, the performance with same parameters, the proposed SMC is better than with a PI controller-based conventional technique.

The inverter voltage and current waveforms for conventional and H7 inverter are shown in Fig. 41.6a, b. It can be observed that there are more distortions in the voltage and current waveforms at lower speeds than with higher speeds with conventional technique, whereas with PI, the distortion in the voltage and current are lesser with SMC. Frequency change in the waveform can be observed with both control schemes. The starting current is high with SMC.

The input to PI or SMC is speed error, and output is reference current. The PI controller input and output waveforms are shown in Fig. 41.7a and with SMC is shown in Fig. 41.7b. It is easily observed with the waveforms with Pi controller,

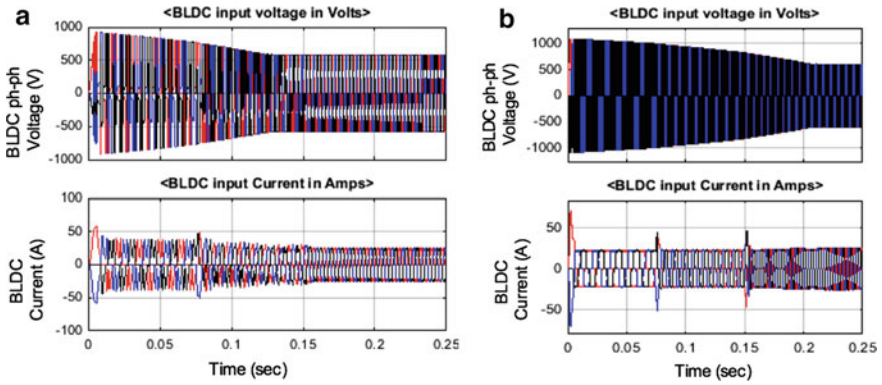

Fig. 41.6 **a** BLDC motor inverter voltage and current with PI controller, **b** with SMC

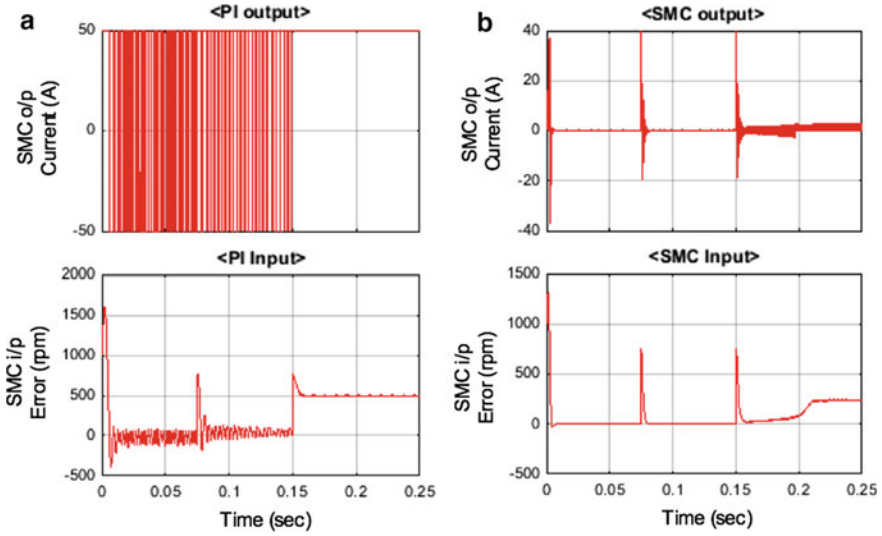

Fig. 41.7 **a** BLDC motor inverter voltage and current with PI controller, **b** with SMC

there are few ripples in the speed error, but is maintained at zero value till the speed is 1750 rpm. But when the speed further increased to a higher value of 2500 rpm, there is deviation in the speed to 500 rpm. However, there are no ripples in the SMC input or speed error value; hence, the desired speed is achieved. But surges are observed when speed change occurred at 0.075 and 0.15 s. When the reference speed is adjusted to 2500, a deviation in the SMC is observed and is around 250 rpm. The current reference value with PI is having large oscillations at lower speed and attained upper saturation value of 50 A when high speed of 2500 rpm is demanded. With SMC, the current reference value or the SMC out value changes considerably when the rotor speed demand changes. There are few spikes in the reference current

value when speed transient occurred. Ripples in current are observed at very higher speed. When speed up to 2280 rpm, the speed deviation is very small with SMC, but beyond this speed, deviation in reference and actual speeds is observed. When compared with works in [30, 31] for BLDC torque ripple reduction, the performance of proposed technique for the BLDC motor is comparatively better with lesser ripples and effective speed and torque control mechanism.

41.5.3 Case C: Variable Torque and Variable Speed Application of BLDC Motor

In this case, both the torque and speed of the solar PV-based BLDC motor are varying and the parameters are observed for the analysis. The motor speed controller is controlled using SMC as shown in Fig. 41.1d. The torque is changing from initial value from 25 to 5 N m at 0.075 s and again increased to 25 N m at 0.15 s and finally reaches to 15 N m at 0.2 s as shown in Fig. 41.8a. The rotor speed reference value is changed from initial value from 1000 rap to 2000 rpm at 0.1 s, and the BLDC motor and the DC link voltage actual waveforms are shown in Fig. 41.8a. It can be observed that starting torque is 45 N m till the rotor speed reaches its reference

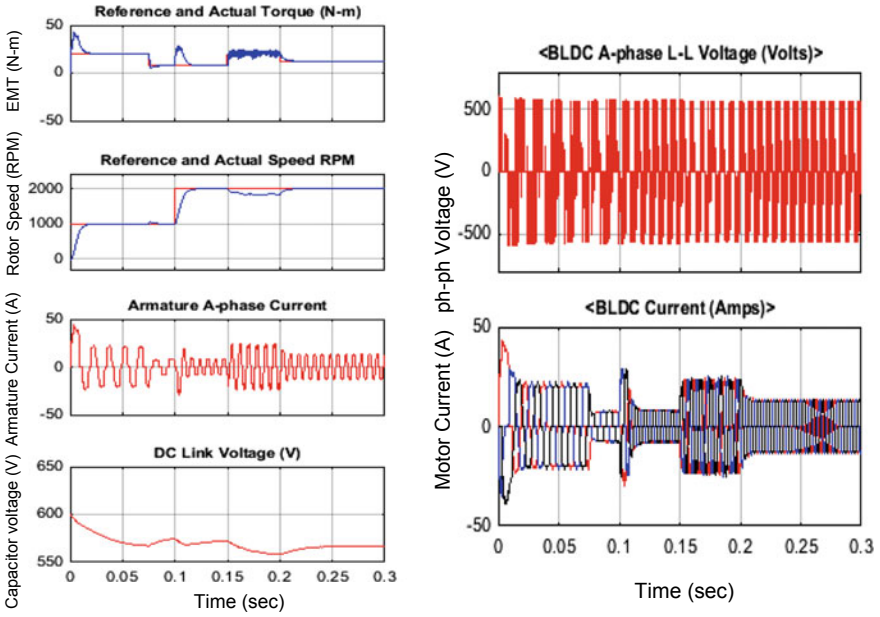

Fig. 41.8 **a** BLDC motor parameters and DC link voltage with SMC, **b** BLDC motor input inverter voltage and current

value of 1000 rpm. There are no ripples in the torque with the proposed method and topology than with a conventional six switch topology.

When the torque is decreased at 0.075 s to 5 N m, there is a small speed change which can be neglected due to the rapid speed controlling action of the SMC. When the rotor speed in increased to twice its value, there is a small surge in the torque and immediately reaches its reference value. With increase in the torque to rated value at rated speed, torque small ripples are observed and small deviation in the rotor speed from 2000 to 1900 rpm due to large load torque application to the motor as shown in Fig. 41.8a. Once the load is decreased by 10 N m to a value of 15 N m, the torque ripples are decreased and the rotor speed also reached its normal value. With the increase in the torque, the armature current is increasing in magnitude, and with increase in the rotor speed, waveform frequency is also increasing, but surges are very less with the proposed scheme and the topology. With the change in the load torque of the motor, the DC link capacitor voltage is also changing, respectively, to supply the desired voltage and current. As there is no chopper control action, the seventh switch only will actively the control the buck and boost action for the inverter.

The BLDC motor voltage source inverter A-phase voltage and three-phase current waveforms are shown in Fig. 41.8b. The voltage magnitude is almost constant but is square wave in shape, and the current magnitude is changing in all the three phases equally in magnitude and frequency with respective change in the torque and the rotor speed. The current waveform is trapezoidal, and there are no surges when torque or speed is changing. The starting current is also high, but the voltage is constant with the proposed control scheme.

The seventh switch location is shown in Fig. 41.1e, and the current through this switch is shown in Fig. 41.9a, and the zoom of the waveform is shown in Fig. 41.9b. The switching current is high when the motor requires high starting current, and this current is very small when there is a decrease in the load torque at 0.075 s. When there is a speed change, the current also is increased till the reference speed is reached. It can also be seen in Fig. 41.9b, the current is almost constant and the switching action is very optimal when H7 topology is used with the proposed control scheme and the SMC proposed controller.

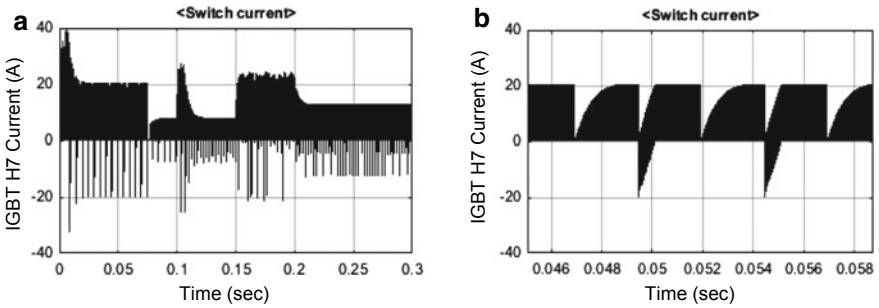

Fig. 41.9 **a** IGBT current through the H7 switch, **b** zoom waveform of IGBT current for (**a**)

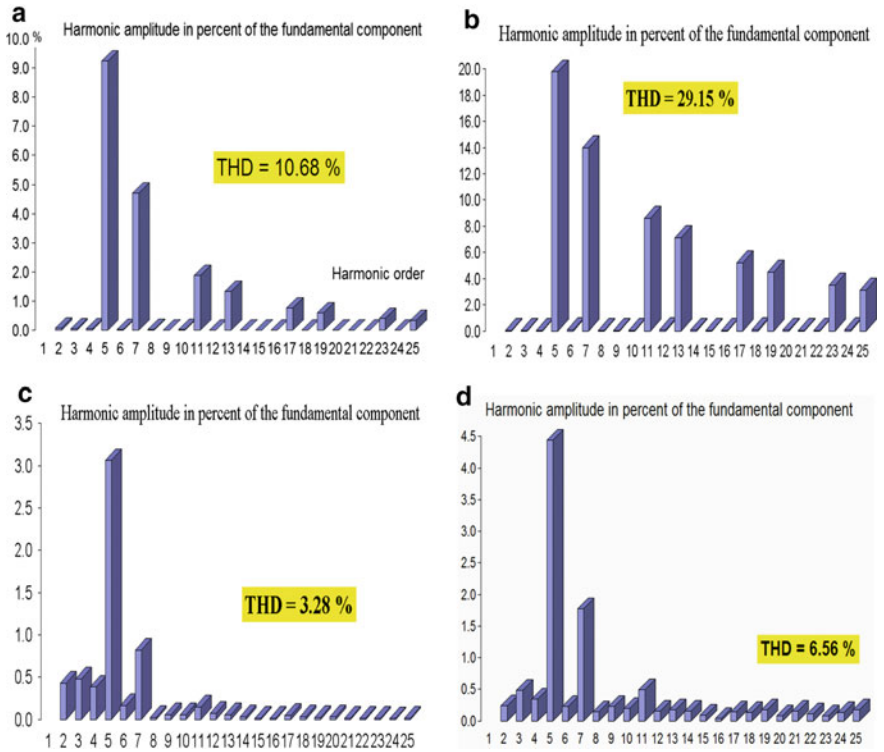

Fig. 41.10 **a** BLDC voltage THD values with SMC controller, **b** With PI controller using H7 inverter topology. **c** BLDC current THD values with SMC controller, **d** with PI controller using H7 inverter topology

The current is having some harmonic components, but the current is in-phase with the same phase voltage. The THD values of current and voltage are shown in Fig. 41.10a, b using PI and SMC controller. The current THD is 10.68%, and voltage is 29.15% with harmonic order of 5, 7, 11, 13, 17, and 19 significant. At full load, the harmonic content of the output current is minimized by the influence of the machine stator equivalent inductance and resistance which are $L_{\_F1} = 3$ mH and $R_{\_S1} = 0.432\ \Omega$, respectively. Unfortunately, this effect is not so noticeable when the available wind decreases and therefore, the maximal output power decreases and the THD increases. The amplitude of the 5th current harmonic is 9.2% of the fundamental, which is greater than the 4% allowed by IEEE 519 standard. Of course, the IEEE 519 standard it is not applicable to this situation but it is a guideline.

The THD presented with the SMC is lower than 3.5% and the low amplitude of the 5th harmonic under 3.5% reveals the suitability of this topology to harmonic mitigation as shown in Fig. 41.11a. An effective improvement in the voltage THD was obtained results which are shown in Fig. 41.11b. These good results were obtained for a constant duty cycle around 50%. The main drawback of this Boost topology is

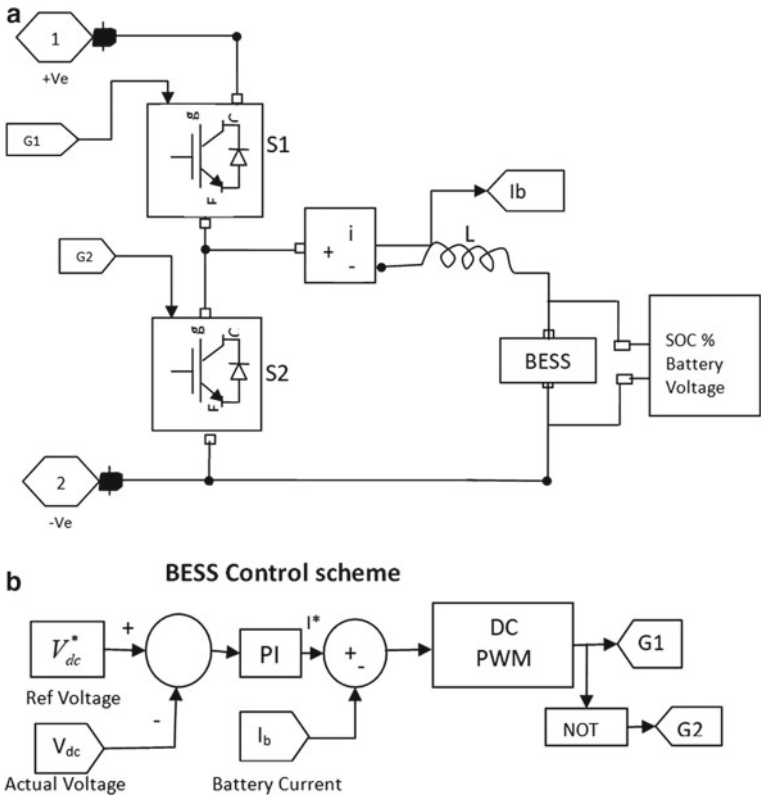

Fig. 41.11 **a(i)** BESS bidirectional current flow circuit configuration for electric vehicle. **a(ii)** BESS bidirectional current control scheme for EV application. **b** BLDC motor parameters and DC link voltage with SMC. **c** BLDC motor input inverter voltage and current

the high output voltage 1 kV, in as much the line-to-line BLDC RMS output voltage has increased to 220 V at full load, and the BLDC line current has decreased once the output power was kept constant at 2 kW. A comparison of the conventional two-stage solar PV inverter, conventional PI controller, and with proposed SMC controller showing different losses and efficiency is denoted in Table 41.3. Compared to the combination, the proposed SMC is better in terms of THD, PFC, and also in terms of efficiency than with PI controller or with a H-bridge two stage converter.

41.5.4 Case D: Application of BLDC Motor as Electrical Vehicle (EV) Load

The same control strategy and H7 topology are applied for battery-based electric vehicle and the performance is observed. In general, the electric vehicle will be a

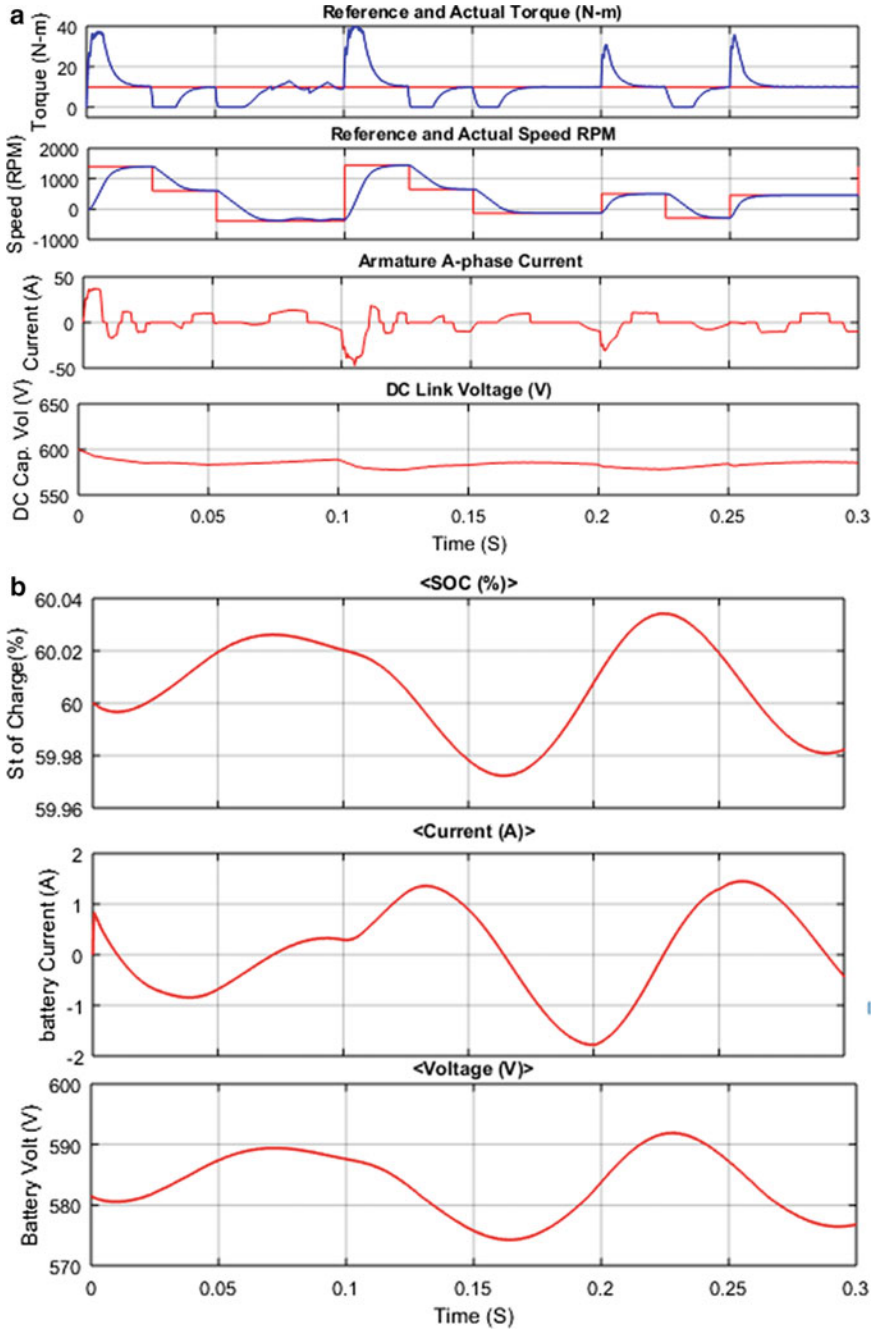

Fig. 41.11 (continued)

Table 41.3 BLDC core, copper, friction, and windage losses in (W) and efficiency in (%)

Topology	Copper losses	Core losses	Friction and windage losses	Cumulative losses	Overall efficiency of the drive
Rated	1701.15	219.40	120	2040.55	90.74
Conventional two stage converter	2318.93	180.82	120	2619.75	88.42
PI-based H7 converter	1724.73	251.32	120	2096.05	90.51
SMC-based H7 converter	1486.33	269.96	120	1876.29	91.42

variable speed and load machine which is based on road and traffic [37]. During the acceleration period, the BLDC-based electric vehicle will receive power from both electrical source and also from the battery based on the charge control scheme state of charge (SOC) of the battery will decrease. Now, when the vehicle is braking, it will decelerate. So, the vehicle decelerating kinetic energy will charge the battery and SOC will increase. The bidirectional current topology is shown in Fig. 41.11a(i), and the battery charge control scheme is shown in Fig. 41.11a(ii). Both the switches ($S1$ and $S2$) are used for bidirectional current flow, and the inductor (L) for smoothening of current.

The control scheme shown in Fig. 41.11a(ii) requires DC link capacitor or bus voltage, battery current measurements. The reference and actual DC link voltages are compared and controlled using a tuned PI controller to get the desired current to be allowed to flow from or to the bus using the battery bank. This reference current is compared with the battery current, and the difference in the current is given to the PWM pulse generation scheme to get the pulses for the two switches. The output of the H7-based BLDC motor as an electrical drive is shown in Fig. 41.11b. Here, the motor speed is before the gear-box, so its speed is nominal speed without decrease in its value. During acceleration, the rotor speed value will be increasing with time, and during deceleration, the rotor speed value is negative in magnitude with the time. During the starting, the vehicle is having good starting torque till its rated speed is reached and later the normal torque is maintained, when the speed is decreasing at 0.025 s, the torque on it is also decreased as can be observed from Fig. 41.11b. When finally brakes are applied at 0.05 s, the torque on it is decreasing and becoming zero, hence no-load type operation where its kinetic energy is delivered to the battery system for energy storage. Similarly, when after stopping and restarting at 0.1 s, its torque is increasing and process is almost the same for the analysis. With the change in the speed of the rotor, the current waveform frequency is varying and because of distortion in the vehicle torque, the current waveform is changing as shown in the figure. Further with the change in the speed and torque values, the DC link voltage is also increasing and decreasing, while the overall value is almost constant. The reference DC link voltage here is 575 volts, based on inverter and the battery ratings.

The battery charging and discharging rates can be observed based on its state of charge (SOC) and the current flow between the battery and the DC bus system. When the motor speed is increasing when starting and also torque is high, the SOC is decreasing and also the current flow is from the battery to aid the vehicle transportation as shown in Fig. 41.11c. When, the vehicle set speed and torque are reached, the SOC and current are also increasing. In the same way, when speed and torque are increasing with time, SOC is decreasing and the battery is supplying as an aid to the grid during the sudden change in the vehicle values.

In the same way, when the speed and torque are decreasing during the vehicle braking operation, the stored kinetic energy in the battery will be dissipated and is charging the battery, and hence, the current flow to the battery is increasing and also the SOC is increasing. The battery voltage is also changing with respect to the current flow in the battery. Hence, overall behavior is improved with the proposed BLDC H7 converter scheme when applied to the electric vehicle application.

41.6 Conclusion

The sliding mode controller (SMC)-based speed error controller and H7-based seven switch inverter topology is considered in this paper for the performance improvement of solar PV-based brushless DC (BLDC) motor. In this, the position sensor and speed are measured in a conventional way using hysteresis sensors. But, topology, control scheme, and SMC scheme are different and are improved. The technique improved the speed and torque control and also effectively curtailed the torque ripples and back-emf waveform when compared to conventional vector control scheme with PI controller. The proposed technique is helpful for high speed up to 2500 rpm and with large motor load torque about 60 N m. The speed and torque surges and ripples are very less. With small-rated DC link capacitor value, the speed and torque control with better waveforms are observed.

The inverter voltage and current waveform are trapezoidal with lesser distortions. This technique is applicable to water pump system and automotive system where load fluctuations and speed variations are more. AS fluctuations in speed and torque are also less, it can be used for emergency systems and advanced control systems like robotic arms and medical applications. Therefore from all the above, the overall performance of BLDC motor is improved with the proposed SMC and H7 inverter topology. The current THD as well as the voltage THD are better with bridgeless ZETA than with the CUK. The same control strategy and topology are applied for the electrical transportation vehicle to observe the effectiveness. It is found that the response of the vehicle with the speed change is quicker, and the battery charging is also effective with the developed algorithm. Even with large speed variations with time considering as acceleration and deceleration, the motor torque is within the range and not going out of step. Also, starting torque is high and the charging and discharging phenomenon of battery is considerably fast.

The overall losses are lesser, and higher efficiency is observed with bridgeless ZETA than with the bridgeless CUK and bridged (H-bridge-based two stage) ZETA is having more losses. Hence in all ways, the bridgeless ZETA is found better and efficient for the BLDC motor drive application. The future scope of the work is to maintain the speed deviation to as low as possible even at higher load torque or rotor speed with limited rating capacitor value.

Appendix

The BLDC parameters: $R_s = 1.8750\ \Omega$, $L_s = 8.5$ mH, flux linkage $= 0.175$, back-emf flat area is 120°, moment of inertia $(J) = 0.8$ m kg m^2, friction coefficient $(F) =$ 1 m N m s, pole pairs $(\rho) = 4$. The SMC parameters constant $C_1 = 9$, C_2 and C_3 are 45, $K = 0.1$ and $\beta = 30$, hysteresis bias $= 0.50$, and DC link capacitor value is 3550 μF.

References

1. B. Banu Rekha, B. Somasundaram, L. Ashok Kumar, P. Balekai, A technical review on advantages of using EC BLDC fans in factory and commercial buildings. Energy Eng. **115**(3), 57–74 (2018)
2. H.A. Toliyat, G.B. Kliman (eds.), *Handbook of Electric Motors*, vol 120 (CRC Press, 2018)
3. J. Shao, An improved microcontroller-based sensorless brushless DC (BLDC) motor drive for automotive applications. IEEE Trans. Ind. Appl. **42**(5), 1216–1221 (2006)
4. D.V.N. Ananth, Performance evaluation of solar photovoltaic system using maximum power tracking algorithm with battery backup, in *PES T&D 2012* (IEEE, 2012), pp. 1–8
5. S.P. Nikam, V. Rallabandi, B.G. Fernandes, A high-torque-density permanent-magnet free motor for in-wheel electric vehicle application. IEEE Trans. Ind. Appl. **48**(6), 2287–2295 (2012)
6. W. Lee, J.H. Kim, W. Choi, B. Sarlioglu, Torque ripple minimization control technique of high-speed single-phase brushless DC motor for electric turbocharger. IEEE Trans. Vehic. Technol. **67**(11), 10357–10365 (2018)
7. J. Feng, K. Liu, Q. Wang, Scheme based on buck-converter with three-phase H-bridge combinations for high-speed BLDC motors in aerospace applications. IET Electric Power Appl. **12**(3), 405–414 (2018)
8. D. Jianwen Shao, M. Nolan, Teissier, D. Swanson, A novel microcontroller-based sensorless brushless DC (BLDC) motor drive for automotive fuel pumps. IEEE Trans. Ind. Appl. **39**(6), 1734–1740 (2003)
9. A.A. El-Samahy, M.A. Shamseldin, Brushless DC motor tracking control using self-tuning fuzzy PID control and model reference adaptive control. Ain Shams Eng. J. **9**(3), 341–352 (2018)
10. K. Premkumar, B.V. Manikandan, Speed control of Brushless DC motor using bat algorithm optimized adaptive neuro-fuzzy inference system. Appl. Softw Comput. **32**, 403–419 (2015)
11. S. Chen, G. Liu, L. Zhu, Sensorless control strategy of a 315 kW high-speed BLDC motor based on a speed-independent flux linkage function. IEEE Trans. Industr. Electron. **64**(11), 8607–8617 (2017)

12. R.L. Valle, P.M. De Almeida, A.A. Ferreira, P.G. Barbosa, Unipolar PWM predictive current-mode control of a variable-speed low inductance BLDC motor drive. IET Electr. Power Appl. **11**(5), 688–696 (2017)
13. D.K. Potnuru, A. Mary, C.S. Babu, Experimental implementation of flower pollination algorithm for speed controller of a BLDC motor. Ain Shams Eng. J. (2019)
14. B.N. Kommula, V.R. Kota, Direct instantaneous torque control of brushless DC motor using firefly algorithm based fractional order PID controller. J. King Saud Univ. Eng. Sci. (2018)
15. A.G. de Castro, W.C.A. Pereira, T.E.P. de Almeida, C.M.R. de Oliveira, J.R.B. de Almeida Monteiro, A.A. de Oliveira, Improved finite control-set model-based direct power control of BLDC motor with reduced torque ripple. IEEE Trans. Ind. Appl. **54**(5), 4476–4484 (2018)
16. Y. Lu, X. Xie, Sliding mode observer of BLDC motor drive under DTC scheme with hall signals, in *Proceedings of the 2018 International Conference on Robotics, Control and Automation Engineering* (ACM, 2018), pp. 60–64
17. A. Alouane, A.B. Rhouma, A. Khedher, FPGA implementation of a new DTC strategy dedicated to delta inverter-fed BLDC motor drives. Electric Power Comp. Syst. **46**(6), 688–700 (2018)
18. G.T.C. Sekhar, B.S. Rao, K.M. Tatikonda, SVPWM-based DTC controller for brushless DC motor, *Computational Intelligence in Data Mining* (Springer, Singapore, 2017), pp. 759–769
19. N. Qamar, C.J. Hatziadoniu, Cancellation of selected stator harmonics in BLDC by using an adaptive feedforward controller. Electr. Power Syst. Res. **154**, 88–94 (2018)
20. M.N. Gujjar, P. Kumar, Comparative analysis of field oriented control of BLDC motor using SPWM and SVPWM techniques, in *2017 2nd IEEE International Conference on Recent Trends in Electronics, Information and Communication Technology (RTEICT)* (IEEE, 2017), pp. 924–929
21. K.D. Carey, N. Zimmerman, C. Ababei, Hybrid field oriented and direct torque control for sensorless BLDC motors used in aerial drones. IET Power Electron. **12**(3), 438–449 (2018)
22. X. Li, C. Xia, Y. Cao, W. Chen, T. Shi, Commutation torque ripple reduction strategy of Z-source inverter fed brushless DC motor. IEEE Trans. Power Electron. **31**(11), 7677–7690 (2016)
23. M. Sumega, Š. Zoššák, P. Varecha, P. Rafajdus, Sources of torque ripple and their influence in BLDC motor drives. Transp. Res. Procedia **40**, 519–526 (2019)
24. H.K.S. Ransara, U.K. Madawala, A torque ripple compensation technique for a low-cost brushless DC motor drive. IEEE Trans. Industr. Electron. **62**(10), 6171–6182 (2015)
25. K. Premkumar, B.V. Manikandan, GA-PSO optimized online ANFIS based speed controller for Brushless DC motor. J. Intell. Fuzzy Syst. **28**(6), 2839–2850 (2015)
26. K. Premkumar, B.V. Manikandan, Stability and performance analysis of ANFIS tuned PID based speed controller for brushless DC motor. Curr. Signal Transduct. Ther. **13**(1), 19–30 (2018)
27. T.V. Krishnan, C.M.C. Dhaneesh, Krishnan, K. Panduranga Vittal, Design of robust H-infinity speed controller for high performance BLDC servo drive, in *2017 International Conference on Smart grids, Power and Advanced Control Engineering (ICSPACE)* (IEEE, 2017), pp. 37–42
28. M.G. López, P. Ponce, L.A. Soriano, A. Molina, J.J.R. Rivas, A novel fuzzy-PSO controller for increasing the lifetime in power electronics stage for brushless DC drives. IEEE Access **7**, 47841–47855 (2019)
29. S.B. Murali, P. Mallikarjuna Rao, Adaptive sliding mode control of BLDC motor using cuckoo search algorithm, in *2018 2nd International Conference on Inventive Systems and Control (ICISC)* (IEEE, 2018), pp. 989–993
30. V. Viswanathan, J. Seenithangom, Commutation torque ripple reduction in the BLDC motor using modified SEPIC and three-level NPC inverter. IEEE Trans. Power Electron. **33**(1), 535–546 (2017)
31. C.K. Lad, R. Chudamani, Simple overlap angle control strategy for commutation torque ripple minimisation in BLDC motor drive. IET Electric Power Appl. **12**(6), 797–807 (2018)
32. A. Soumi, A. Prince, A novel approach of sensorless control of BLDC motor with Z-source inverter. J. Power Electron. Power Syst. **8**(3), 9–16 (2018)

33. M. Jagiela, T. Garbiec, J. Gwozdz, J. Kolodziej, Fast steady-state field-circuit model for SMPM-BLDC motors driven from 120 and 180 quasi-square wave inverters. IEEE Trans. Magnetic. **52**(3), 1–4 (2015)
34. H. Suryoatmojo, A.P. Nandiwardhana, N.R. Arsya, S. Anam, H.P. Putra, R. Mardiyanto, M. Ashari, Comparisons of Cuk, SEPIC and Zeta converter performance for harmonics mitigation and PFC in BLDC speed control, in *2016 International Seminar on Intelligent Technology and Its Applications (ISITIA)* (IEEE, 2016), pp. 681–686
35. A.J. Garrido, M.A. IzaskunGarrido, M. Alberdi, M. De la Sen, Sliding-mode control of wave power generation plants. IEEE Trans. Ind. Appl. **48**(6), 2372–2381 (2012)
36. T.K. Freddy, N.A. Rahim, W.-P. Hew, H.S. Che, Modulation techniques to reduce leakage current in three-phase transformerless H7 photovoltaic inverter. IEEE Trans. Industr. Electron. **62**(1), 322–331 (2014)
37. J. Liu, C. Tong, Z. Jin, G. Qiao, P. Zheng, Research on system control and energy management strategy of flux-modulated compound-structure permanent magnet synchronous machine. CES Trans. Electr. Mach. Syst. **1**(2), 100–108 (2017)